Disturbance Rejection in Space Applications: Problems and Solutions

in Acta Astronautica 72 (2012) 121–131

# Disturbance rejection in space applications: Problems and solutions

Enrico Canuto*, Andrés Molano-Jimenez, Carlos Perez-Montenegro

*Politecnico di Torino, Dipartimento di Automatica e Informatica, Corso Duca degli Abruzzi 24, 10129 Torino, Italy*

A B S T R A C T

Navigation, control and guidance of the propulsive phase of planetary landing, e.g. on Mars (or the Moon), with a soft landing being the only target, are driven by Inertial Measurement Units and a radar altimeter/velocimeter. Their measurements are affected by bias and scale errors. The latter ones are aggravated by the attitude navigation error as it accumulates during the ballistic (and aerodynamic) flight after orbiter separation and couples for most of the descent trajectory with the vehicle axis inclination from the local vertical direction. By complementing the center-of-mass dynamics with appropriate disturbance state equations driven by noise vectors and estimating the noise from the model error (plant measurements minus model output), scale errors and bias can be retrieved in real time in the form of disturbance state variables. Although a similar complement is adopted in the standard navigation algorithms, it takes the form of an output disturbance, which may lead to unobservability. In this paper instead, the disturbance complement is designed to be fully observable, which may require that the derivatives of smooth systematic errors be pushed up to the command channel (a form of back-stepping). It is then viable, unlike standard navigation, to eliminate them from position and velocity tracking errors through disturbance rejection, under appropriate convergence conditions and sensor layout. It will, however, be demonstrated in this paper that the same result cannot be achieved under pure feedback control. Since constant errors (bias) become zero through back-stepping, a well known fact derives: bias can only be eliminated by disposing of supplementary sensors.

To further enlighten and solve the question of bias rejection, a further case study is treated. The attitude control of drag-free satellites is considered, where fine accelerometers allow for the rejection of wide-band aerodynamic torques (think of low-Earth orbit spacecrafts) at the price of attitude divergence because of accelerometer bias and drift. The spacecraft attitude can be made bounded and accurate, if bias and drift are modeled as angular accelerations, affecting the attitude. They are estimated by attitude sensors like star trackers and then are rejected by the attitude control. The results in the soft landing and drag free case studies are illustrated by simulated runs and Monte Carlo trials.

## 1. Introduction

Elimination of sensor bias and scale errors (in general of systematic errors) from tracking errors is discussed as a case study in disturbance rejection and space applications. Systematic errors affect the 'true' variable to be controlled, biasing the tracking error, which is the difference between the reference and the 'true' variable. Biasing cannot be accepted if significant compared to zero-mean fluctuations caused by random sources. Therefore, calibration must be performed, either off-line or on-line [1–7].

On-line calibration is usually performed though different versions and extensions of the Kalman filter, starting from Friedland's paper [4]. A classical problem is the bias and scale factor estimation of the different sensors to be

* Corresponding author. Tel.: +39 011 564 7026; fax: +39 011 564 7198

*E-mail address:* enrico.canuto@polito.it (E. Canuto).

integrated in a navigation process [7], which is the same problem dealt with herein. Navigation is performed as a stand-alone process fully separated from control law, though feeding the latter. Stand-alone navigation is permitted by accelerometer units that provide the external accelerations (disturbance and command) acting on the body. Integrating the acceleration provides the navigation state variables, velocity and position. Drift, provoked by accelerometer errors, can be corrected provided velocity and position measurements are available. The correction scheme is usually implemented as a Gauss–Markov estimator, as in Kalman filtering. Error statistics must be propagated to the purpose. Systematic errors are usually modeled as a first order random drift adding to the measured variable in the form of an output disturbance. A key problem is the observability of the output disturbance, which is usually guaranteed by supplementary and appropriate sensors. The observability problem is not explicitly dealt with in [4–6] but is mentioned in [7]. The filtering objective is to provide control strategies with state variables (velocity and position) free from drift or systematic errors, when the latter ones are observable.

The same problem is faced here in a different and more generic manner. Firstly, acceleration is split into command and input disturbance and the dynamics of the latter is explicitly modeled. The advantage is to allow commands to explicitly contrast not only gravity, but also aerodynamic forces. Secondly, systematic errors are treated as a particular case of output disturbance as in the aforementioned standard navigation scheme; yet the observable components are not simply estimated, but rejected through a control law. This implies that the controlled variable is no longer the 'true' variable which is measured, but rather a 'dirty' variable sum of the 'true' variable and of systematic errors. A new control problem arises, and the interest is to prove under which conditions the zero tracking error of a 'dirty' variable is paralleled by the zero tracking error of the 'true' variable. Rejection of the output disturbance is a well known problem in classical and modern control [8,9], usually solved via the internal model principle, where a disturbance is modeled as the free response of a linear and time invariant state equation and a servo-compensator is designed as in [8].

One advantage of the present approach is to embed navigation in the whole control algorithm, as it is suggested by the Embedded Model Control [10–12]. Guidance (reference generator), navigation and control are designed around a unique dynamic model, the embedded model, which is the core of the control unit, made up of two parts, controllable and disturbance dynamics. The former is driven by commands, the latter by a noise vector playing the role of a disturbance input, to be real-time retrieved from the model error (plant output less model output) by means of a suitable noise estimator. The free response of the disturbance dynamics describes 'known components' that must not be real-time retrieved. The ensemble of embedded model and noise estimator becomes the navigation filter (actually a state predictor) affected by prediction errors.

As a property of the embedded model, all the state variables, forced either by command, or noise, must be observable from the model output. The restriction implies that systematic errors cannot be modeled as the output of a dynamic system whose eigenvalues are equal to those of the controllable dynamics. In fact, adding the systematic error to the 'true' variable makes the overall system unobservable, or, equivalently, the state equation non-minimal. The remedy is to minimize the state variables by 'back-stepping' the output disturbance up to the command location. In other words, it amounts to replacing systematic errors with their derivatives, as in feedback linearization [13]. Error derivatives must exist, which is coherent with systematic error smoothness. Naturally, some limitations may occur since derivation can force some error components, such as bias, to zero. Indeed, the latter need not be back-stepped, but requires supplementary sensors to become 'real-time' observable. The observable disturbance can then be rejected by a control law, freeing the 'dirty' variable from systematic errors, less prediction errors. No supplementary sensor is necessary since systematic errors are only eliminated from the 'dirty' variable and not from the 'true' one. The correction becomes effective when the reference trajectory to be tracked converges to a condition of zero systematic error, as in the planetary soft landing case dealt with in this paper. In that case, the 'true' variable converges to the 'dirty' one, and, therefore, to the reference trajectory, as will be demonstrated further on.

Methods and results are outlined with the help of simple case studies derived from space applications. No general formulation is carried out in this paper. The first problem concerns planetary soft landing [14] when the powered descent is driven by inertial measurements (100 Hz accelerometers and gyros) complemented with radar altimeter and velocimeter data (usually available at a rate between 10 and 20 Hz). Without loss of generality, the treatment in Sections 2 and 3 will assume a common rate. Since attitude is propagated from gyro measurements, its uncertainty affects velocity and altitude measurements with a scale error as they are converted from the body to the local vertical local horizontal frame, where the descent command is computed. The same goes for accelerometer measurements. Moreover, all the measurements are affected by bias.

Firstly, a 3D velocity control shows how accelerometer errors can be fully eliminated throughout the whole of the descent phase, whereas velocimeter errors are progressively eliminated, less the bias, as soon as the velocity magnitude tends to zero. Then a single degree-of-freedom altitude control is outlined, proving that accelerometer and velocimeter errors are eliminated throughout the whole of the descent phase, whereas altimeter errors tend to zero less the bias as soon as the velocity magnitude approaches zero. In soft landing, only vertical position is controlled. Discrete time is adopted.

The second application is the 10 μrad attitude control of a drag-free satellite endowed with ultra-fine 10 Hz accelerometers providing center-of-mass (CoM) and angular accelerations [11]. These are essential for a wide-band rejection (up to 0.5 Hz) of aerodynamic, magnetic and gravity accelerations well below 0.1 $\mu rad/s^2$. Accelerometer bias, though very small, is such to make the attitude drifting out of milliradians in a few tens of seconds. Endowing the

spacecraft with star trackers, though sampled at a rate not greater than 2 Hz and affected by an equivalent noise larger than 20 μrad (1 sigma), allows the accelerometer bias to be compensated for and the reference attitude to be accurately tracked.

## 2. Soft landing velocity control

Soft landing requires that the velocity magnitude $v=|\mathbf{v}|$ be brought to zero and the vehicle axis tends to be vertical at the terminal time $t_f$ corresponding to a pre-specified altitude $h_f$ from ground. If touch-down is softened either by air bags, crushable structures (ExoMars landing demonstrator [15]), or damping legs, then the thrusters controlling the vehicle braking are switched off at $t_f$. If the vehicle landing is planned in such a way that it is to hover over the landing site, such as in the case of the US Mars Science Laboratory [16], thrust is lowered so as to simply compensate for local gravity.

### 2.1. State equations

Denote the center-of-mass velocity coordinates in the local vertical local horizontal frame (assumed to be inertial) with the three-dimensional vector $\mathbf{v}$, and write the CoM dynamics as

$$\begin{aligned}&\mathbf{v}(i+1)=\mathbf{v}(i)+\mathbf{a}_u(i)+\mathbf{d}(i)+\mathbf{w}_u(i)-\mathbf{g}(i)\\&\mathbf{d}(i+1)=\mathbf{d}(i)+\mathbf{w}_d(i)\\&\mathbf{y}_v(i)=\mathbf{v}(i)+\mathbf{s}_v(\mathbf{v}(i))+\mathbf{e}_v(i),\end{aligned}\tag{1}$$

where $i$ is the discrete-time instant corresponding to a time unit $T=0.05$ s, $\mathbf{d}$ is a disturbance state mainly accounting for aerodynamic forces, $\mathbf{w}_u$ and $\mathbf{w}_d$ are noise vectors, $\mathbf{a}_u$ is the commanded acceleration, $\mathbf{y}_v$ is the velocimeter measurement affected by the systematic error $\mathbf{s}_v$ and the model error $\mathbf{e}_v$, and $\mathbf{g}$ is the known gravity vector. All the vectors in (1) are three-dimensional. The concept of a model error like $\mathbf{e}_v$ affecting the measured variable $\mathbf{y}_v$ [10] is more generic than that of measurement error, as it includes the effect of the input-output dynamics (actuator and sensor) which has been neglected in (1). Since sensor and actuator dynamics are not dealt with in this paper, model error coincides with measurement error. Random errors and noises may be modeled either as discrete-time white noises, or as zero-mean bounded, arbitrary signals. The systematic error is a smooth function of $\mathbf{v}$. For simplicity's sake a first order disturbance dynamics has been written in (1). Smoothness assumption on $\mathbf{s}_v$ implies the existence of the difference equation

$$\mathbf{s}_v(i+1)-\mathbf{s}_v(i)=S_v(\tilde{\mathbf{v}}(i))(\mathbf{v}(i+1)-\mathbf{v}(i))=S_v(\tilde{\mathbf{v}}(i))\mathbf{a}(i),\tag{2}$$

where $S_v$ is the Jacobian matrix of $\mathbf{s}_v(\mathbf{v}(i))$ and is computed at the interpolated velocity $\tilde{\mathbf{v}}(i)=\alpha(i)\mathbf{v}(i)+(1-\alpha(i))\mathbf{v}(i+1)$, $0\le\alpha\le1$, so as to guarantee equality in (2). In the velocimeter case, the Jacobian matrix holds $S_v=\Delta S+\Delta R_b(i)$, where $\Delta S$ is the constant scale error matrix including misalignments, whereas $\Delta R_b$ is the transformation error from body to inertial frame. The latter matrix typical bound is $|\Delta R_b|\le0.05$ rad. The following result states that the systematic error $\mathbf{s}_v$ is not observable from (1) and (2).

*Result 1.* The state variables in (1) and (2) are not observable from $\mathbf{y}_v$.

The proof comes by observing that $\mathbf{s}_v$ and $\mathbf{v}$ sum up in the output equation of (1) and belong to the state equations (1) and (2) having equal and unitary eigenvalues.

Observability can be recovered by rewriting (1) and (2) in terms of the 'dirty' velocity

$$\mathbf{v}_d=\mathbf{v}+\mathbf{s}_v,\tag{3}$$

and of the 'extended' disturbance

$$\mathbf{d}_v=\mathbf{d}+S_v\mathbf{a}.\tag{4}$$

In other terms, $\mathbf{s}_v$ has been dropped from the output Eq. (1) and 'back-stepped' to become an acceleration disturbance, thus converting (1) into the state equations

$$\begin{aligned}&\mathbf{v}_d(i+1)=\mathbf{v}_d(i)+\mathbf{a}_u(i)+\mathbf{d}_v(i)+\mathbf{w}_u(i)-\mathbf{g}(i)\\&\mathbf{d}_v(i+1)=\mathbf{d}_v(i)+\mathbf{w}_d(i)\\&\mathbf{y}_v(i)=\mathbf{v}_d(i)+\mathbf{e}_v(i),\end{aligned}\tag{5}$$

which are now observable.

As a proof guideline, rewriting (3) as $\mathbf{v}=\mathbf{v}_d-\mathbf{s}_v$ and replacing the same equation in (1) yields

$$\begin{aligned}&\mathbf{v}_d(i+1)=\mathbf{v}_d(i)+\mathbf{a}_u(i)+\mathbf{d}(i)+\mathbf{s}_v(i+1)-\mathbf{s}_v(i)+\mathbf{w}_u(i)-\mathbf{g}(i)\\&\mathbf{y}_v(i)=\mathbf{v}_d(i)+\mathbf{e}_v(i).\end{aligned}\tag{6}$$

Then, Eq. (5) follows by replacing $\mathbf{d}(i)+\mathbf{s}_v(i+1)-\mathbf{s}_v(i)$ in (6) with the help of (2) and (4), and by assigning $\mathbf{d}_v(i)$ the same state equation of $\mathbf{d}(i)$ in (1). The latter stage assumes that any realization of $S_v\mathbf{a}$ (the back-stepped systematic error) is sufficiently approximated by the realizations of a 1st order random drift driven by $\mathbf{w}_d$ as in (5). The assumption can be reinforced by interpreting a random drift as an arbitrary step-wise function [10], which is coherent with the expected time profile of $S_v\mathbf{a}$. Indeed, $\mathbf{a}(i)$ in (4) approaches a step-wise profile since it corresponds to the constant deceleration forcing $\mathbf{v}$ to zero (see Fig. 1).

### 2.2. Accelerometer measurements and observability

Because of a wider bandwidth and a lower noise, $\mathbf{d}_v$ in (5) can be better retrieved from accelerometer measurements. For simplicity's sake, the measurements are assumed to be sampled at the same rate $1/T$ of the velocimeter. A multi-rate case, not essential here, is treated in Section 4. State and output equations are as follows:

$$\begin{aligned}&\mathbf{x}_a(i+1)=A\mathbf{x}_a(i)+\mathbf{a}(i)+\mathbf{s}_a(i)+\mathbf{w}_a(i)\\&\mathbf{s}_a(i+1)=\mathbf{s}_a(i)+\mathbf{w}_s(i)\\&\mathbf{y}_a(i)=\mathbf{x}_a(i)+\mathbf{e}_a(i)\\&\mathbf{a}(i)=\mathbf{a}_u(i)+\mathbf{d}(i)+\mathbf{w}_u(i).\end{aligned}\tag{7}$$

In (7) all the vectors are three-dimensional, $\mathbf{x}_a$ plays the role of a 'dirty' acceleration, $\mathbf{a}$ is the 'true' acceleration already used in (4), $\mathbf{s}_a$ is the systematic error including scale error, bias and drift, $\mathbf{w}_a$ and $\mathbf{e}_a(i)$ are random errors. The $3\times3$ state matrix $A$ accounts for the accelerometer dynamics, which, though usually neglected, is not here as it converts measurement errors into disturbances. In the simplest case, dynamics reduces to a single delay, in which case $A=0$ as assumed here.

In standard navigation, the accelerometer dynamics is neglected and (7) is replaced by

$$\begin{aligned}&\mathbf{y}_a(i)=\mathbf{a}(i)+\mathbf{s}_a(i)+\mathbf{w}_a(i)\\&\mathbf{s}_a(i+1)=\mathbf{s}_a(i)+\mathbf{w}_s(i)\\&\mathbf{a}(i)=\mathbf{a}_u(i)+\mathbf{d}(i)+\mathbf{w}_u(i).\end{aligned}\tag{8}$$

Then solving (8) for $\mathbf{a}(i)$ and replacing the solution in (5), the second order navigation equation is found

$$\begin{aligned}&\mathbf{v}_d(i+1)=\mathbf{v}_d(i)+\mathbf{y}_a(i)-\mathbf{s}_a(i)-\mathbf{w}_a(i)-\mathbf{g}(i)\\&\mathbf{s}_a(i+1)=\mathbf{s}_a(i)+\mathbf{w}_s(i)\\&\mathbf{y}_v(i)=\mathbf{v}_d(i)+\mathbf{e}_v(i),\end{aligned}\tag{9}$$

where $\mathbf{y}_a$ and $\mathbf{g}$ are known input signals, $\mathbf{d}_v$ disappears and only $\mathbf{s}_a$ plays a disturbance role. Since (9) is observable, the simple noise estimator

$$\begin{bmatrix}\mathbf{w}_a\\ \mathbf{w}_s\end{bmatrix}(i)=\begin{bmatrix}L_a\\ L_s\end{bmatrix}(\mathbf{y}_v-\mathbf{v}_d)(i)\tag{10}$$

applies, and the gain matrices $L_a$ and $L_s$ can be designed as in Kalman filter. Notice that (9) is still written in terms of the 'dirty' velocity $\mathbf{v}_d$, implying that $\mathbf{s}_a$ is affected by the back-stepped velocimeter error. Departing from standard navigation, the following result states that both the accelerometer error $\mathbf{s}_a$ and the disturbance $\mathbf{d}_v$ are observable.

*Result 2.* The state variables in (5) and (7) are observable from $\mathbf{y}_v$ and $\mathbf{y}_a$.

As a concise proof, (5) and (7) have independent measurements and each one is observable.

### 2.3. Noise estimator

Unlike (9), the ensemble of (5) and (7) leads to a multivariate noise estimation. Exploiting the different bandwidth and noise of accelerometer and velocimeter, a decoupled state predictor is designed as in [11], where the accelerometer model error $\mathbf{e}_a=\mathbf{y}_a-\mathbf{x}_a$ is the source of the noise vectors in (7), and the velocimeter model error $\mathbf{e}_v=\mathbf{y}_v-\mathbf{v}_d$ is the source of the noise vectors in (5). To this end, (5) and (7) are rearranged into a unique state equation as follows:

$$\begin{aligned}&\mathbf{v}_d(i+1)=\mathbf{v}_d(i)+\mathbf{a}_u(i)+\mathbf{d}_s(i)+\mathbf{w}_u(i)+\mathbf{d}_a(i)-\mathbf{g}\\&\mathbf{d}_s(i+1)=\mathbf{d}_s(i)+\mathbf{w}_s(i)\\&\mathbf{x}_a(i+1)=\mathbf{a}_u(i)+\mathbf{d}_a(i)+\mathbf{w}_a(i)\\&\mathbf{d}_a(i+1)=\mathbf{d}_a(i)+\mathbf{w}_d(i),\end{aligned}\tag{11}$$

upon definition of a pair of new disturbance state variables

$$\begin{aligned}&\mathbf{d}_a=\mathbf{d}+\mathbf{s}_a\\&\mathbf{d}_s=S_v\mathbf{a}-\mathbf{s}_a.\end{aligned}\tag{12}$$

The former vector in (12), $\mathbf{d}_a$, sums aerodynamic accelerations and the accelerometer systematic error, whereas $\mathbf{d}_s=S_v\mathbf{a}-\mathbf{s}_a$ sums the opposite of the accelerometer systematic error and the back-stepped velocimeter error.

Decoupling of the noise estimator to be formulated below, is driven by three properties of the Eq. (11).

(1) Firstly, the accelerometer systematic error, though contributing to $\mathbf{d}_a$, has no effect on the total disturbance $\mathbf{d}_s+\mathbf{d}_a$ to be rejected by the command $\mathbf{a}_u$, which implies that the error is implicitly canceled.

(2) Secondly, the noise vectors $\mathbf{w}_u$ and $\mathbf{w}_s$ only affect the velocimeter measurement $\mathbf{y}_v$ and the relevant model error $\mathbf{e}_v$. The only source of their estimation is, accordingly, $\mathbf{e}_v$. A similar reasoning applies to $\mathbf{w}_a$ only affecting $\mathbf{y}_a$.

(3) The third property concerns $\mathbf{w}_d$, which affects both $\mathbf{y}_v$ and $\mathbf{y}_a$ and, in principle, could be estimated by combining $\mathbf{e}_v$ and $\mathbf{e}_a$. Given the time unit $T$ defined in Section 2.1, the dimensionless noise ratio

$$\rho_{av}=\frac{\sigma_a T}{\sigma_v}<0.001,\tag{13}$$

between the accelerometer and velocimeter standard deviations $\sigma_a$ and $\sigma_v$, respectively, is so small that the gain of $\mathbf{e}_v$ can be neglected in a Gauss–Markov estimate. It may be argued that correlated residuals of the estimate of $\mathbf{w}_d$ which is obtained from $\mathbf{e}_a$ alone, could, in turn, be fit by $\mathbf{e}_v$. In fact, by estimating $\mathbf{w}_d$ at a sampling rate higher than the velocimeter, the contribution of $\mathbf{e}_v$ can be made ineffective by a residual correlation vanishing within the velocimeter sampling time. Accelerometer higher rates always occur in practice and it is possible to make the residual correlation vanish by providing a sufficiently wide bandwidth to the closed-loop state predictor from $\mathbf{y}_a$ to $\mathbf{x}_a$.

In the end, the noise vectors in (11) are estimated by the decoupled static feedback laws

$$\begin{aligned}&\mathbf{w}_u(i)=L_u\mathbf{e}_v(i),\quad \mathbf{w}_s(i)=L_s\mathbf{e}_v(i)\\&\mathbf{w}_a(i)=L_a\mathbf{e}_a(i),\quad \mathbf{w}_d(i)=L_d\mathbf{e}_a(i).\end{aligned}\tag{14}$$

The diagonal gain matrices $L_u$, $L_s$, $L_a$ and $L_d$ in (14) are fixed by closed-loop eigenvalues: slower eigenvalues apply to $L_u$ and $L_s$ because of the larger velocimeter noise, and faster ones to $L_a$ and $L_d$ in agreement with a wider bandwidth of the accelerometer state predictor that is made possible by a smaller noise. Decoupling can be shown to approach optimality, under suitable closed-loop eigenvalue selection.

### 2.4. Control law and tracking errors

Neglecting prediction errors in (11), i.e. assuming the noise vectors are exactly retrieved by (14), the control law is designed to force the 'dirty' velocity tracking error $\underline{\mathbf{e}}_v=\underline{\mathbf{v}}-\mathbf{v}_d$ to be bounded. Guidance provides the reference velocity and the acceleration command satisfying

$$\begin{aligned}&\underline{\mathbf{v}}(i+1)=\underline{\mathbf{v}}(i)+\underline{\mathbf{a}}(i)\\&\underline{\mathbf{v}}(t_f)=0,\quad \underline{\mathbf{a}}_u(i)=\underline{\mathbf{a}}(i)+\mathbf{g}(i),\end{aligned}\tag{15}$$

where gravity compensation has been added. Due to command one-step prediction, only disturbance state variables in (11) can be rejected as follows:

$$\mathbf{a}_u(i)=\underline{\mathbf{a}}_u(i)+K_v(\underline{\mathbf{v}}(i)-\mathbf{v}_d(i))-\mathbf{d}_s(i)-\mathbf{d}_a(i),\tag{16}$$

where the sum $\mathbf{d}_s+\mathbf{d}_a$ cancels the accelerometer systematic error, as already anticipated. The following result is proved.

*Result 3.* Control law (16) and guidance (15) if applied to (11) yield the tracking error equation

$$\underline{\mathbf{e}}_v(i+1) = (I-K_v)\underline{\mathbf{e}}_v(i) - \mathbf{w}_u(i), \tag{17}$$

which under asymptotically stable $I-K_v$ and bounded $\mathbf{w}_u(i)$ ensures a bounded error. Moreover assuming $E\{\mathbf{w}_u\}=0$, we have $\lim_{i\to\infty} E\{\underline{\mathbf{e}}_v(i)\} = 0$.

As a concise proof, replace (16) into the top equation of (11) thus canceling $\mathbf{d}_a+\mathbf{d}_s$. Then subtract the remaining equation from (15), thus canceling $\underline{\mathbf{a}}_u$ which results in (17).

The covariance matrix $\underline{P}_e(i)$ of $\underline{\mathbf{e}}_v(i)$ can be obtained from (17) through the asymptotically converging Lyapunov equation

$$\underline{P}_e(i+1) = (I-K_v)\underline{P}_e(i)(I-K_v)^T + W_u, \quad \underline{P}_e(0) = \underline{P}_{e0}, \tag{18}$$

where $W_u$ is the noise steady covariance.

Notice that (17) is linear and time-invariant, as it does not depend on the systematic errors $\mathbf{s}_a$ and $\mathbf{s}_v$. The next step is to extend Result 3 to the 'true' tracking error $\underline{\mathbf{v}}-\mathbf{v}$.

The next result first shows that the 'true' velocity $\mathbf{v}$ asymptotically tends to the reference $\underline{\mathbf{v}}$ under zero reference and unbiased systematic error. Second, it shows that the asymptotic covariance matrix defined by

$$P_v(i) = \lim_{i\to\infty} P_v(i) = E((\mathbf{v}(i)-\boldsymbol{\mu}_v(i))(\mathbf{v}(i)-\boldsymbol{\mu}_v(i))^T)$$
$$\boldsymbol{\mu}_v(i) = E(\mathbf{v}(i)), \tag{19}$$

approaches the asymptotic limit of (18). To this end, (3) is rewritten as

$$\mathbf{v} = \mathbf{v}_d - \mathbf{b}_v - \mathbf{s}_v(\mathbf{v}_d), \quad \mathbf{s}_v(0) = 0$$
$$\mathbf{s}_v(\mathbf{v}_d) = S_v(\tilde{\mathbf{v}})\underline{\mathbf{e}}_v, \quad \tilde{\mathbf{v}} = \underline{\mathbf{v}} - \alpha\underline{\mathbf{e}}_v, \quad 0 \le \alpha \le 1 \tag{20}$$

where $\mathbf{b}_v$ is the velocimeter bias and $\mathbf{s}_v$ has been expanded around $\underline{\mathbf{v}}$.

*Result 4.* Under the conditions (i) $\lim_{i\to\infty} E\{\underline{\mathbf{e}}_v(i)\} = 0$ guaranteed by Result 3, (ii) $\lim_{i\to\infty} \underline{\mathbf{v}}(i) = 0$ corresponding to an asymptotically zero reference, (iii) $|S_v(0)| \le S_{v,\max} \ll 1$ in (20), and denoting the asymptotic covariance of $\underline{\mathbf{e}}_v$ in (18) with $\underline{P}_e$, the following limits hold

$$\lim_{i\to\infty} E\{\mathbf{v}(i)\} = \lim_{i\to\infty} \boldsymbol{\mu}_v(i) = -\mathbf{b}_v$$
$$P_v = (I+S_{v,\max})^{-1}\underline{P}_e(I+S_{v,\max})^{-T} \cong \underline{P}_e \tag{21}$$

*Proof.* The proof of the first limit in (21) follows from taking the asymptotic limit of the expected value in (20), i.e.

$$\lim_{i\to\infty} E\{\mathbf{v}(i)\} = \lim_{i\to\infty} (\underline{\mathbf{v}}(i) + E\{\underline{\mathbf{e}}_v(i)\} - \mathbf{b}_v - E\{S_v(\tilde{\mathbf{v}})\underline{\mathbf{e}}_v(i)\}) = \mathbf{b}_v. \tag{22}$$

The second limit follows from (20) and from the asymptotic equality

$$\lim_{i\to\infty} (\mathbf{v}(i) - \boldsymbol{\mu}_v(i)) = \lim_{i\to\infty} -(I+S_v(\alpha\underline{\mathbf{e}}_v))\underline{\mathbf{e}}_v(i). \tag{23}$$

Assuming $S_v(-\alpha\underline{\mathbf{e}}_v) \cong S_v(0)$ in (23) and the inequality $|S_v(0)| \le S_{v,\max} \ll 1$, the second limit in (21) is proved. □

In the case of planetary landing, Result 4 must be extended to a finite time $t_f = i_f T$.

*Result 5.* If $E\{\underline{\mathbf{e}}_v(i_f)\} = \varepsilon$, $\underline{\mathbf{v}}(i_f) = 0$, and $|S_v(|\varepsilon|)| \le S_{v,\max}$, the following limit holds

$$|\mathbf{b}_v| - (1+S_{v,\max})|\varepsilon| \le |E\{\mathbf{v}(i_f)\}| \le |\mathbf{b}_v| + (1+S_{v,\max})|\varepsilon|. \tag{24}$$

The proof follows by rewriting (20) at $i = i_f$ as follows

$$E\{\mathbf{v}(i_f)\} + \mathbf{b}_v = -(E\{\underline{\mathbf{e}}_v(i_f)\} + E\{S_v(-\alpha\varepsilon)\underline{\mathbf{e}}_v(i_f)\}). \tag{25}$$

Taking the absolute value of (25) and using the assumptions of Result 5, the following inequality is obtained

$$|E\{\mathbf{v}(i_f)\} + \mathbf{b}_v| \le |S_v(|\varepsilon|)|\,|E\{\underline{\mathbf{e}}_v(i)\}| + |\varepsilon|, \tag{26}$$

which proves the result.

### 2.5. Output feedback

Assume the control law (16) does not include any disturbance rejection and the tracking error includes the velocity measurement as follows:

$$\mathbf{a}_u(i) = \underline{\mathbf{a}}_u(i) + K_v(\underline{\mathbf{v}}(i) - \mathbf{y}_v(i)). \tag{27}$$

In fact, $\mathbf{y}_v$ should be filtered from the velocimeter noise as in the standard navigation algorithm consisting of (9) and (10), and of a computing procedure of the gain matrices in (10). Assuming that the velocimeter noise filter leads to the equality $\mathbf{y}_v = \mathbf{v}_d$, then the state equation of the tracking error $\underline{\mathbf{e}}_v = \underline{\mathbf{v}} - \mathbf{v}_d$ holds

$$\underline{\mathbf{e}}_v(i+1) = (I-K_v)\underline{\mathbf{e}}_v(i) - \mathbf{d}(i) - S_v\mathbf{a}(i) - \mathbf{w}_u(i). \tag{28}$$

*Result 6.* Under the same conditions of the Result 4 and using (28), the 'true' velocity asymptote holds

$$\lim_{i\to\infty} E\{\mathbf{v}(i)\} = -\mathbf{b}_v - \lim_{i\to\infty} K_v^{-1} E\{\mathbf{d}(i) + S_v\mathbf{a}(i)\}. \tag{29}$$

The asymptote in (29) cannot be generically zero, which is especially true at a finite time. Also in the case of zero convergence, i.e. when $\mathbf{b}_v = 0$ and $E\{\mathbf{d}(i) + S_v\mathbf{a}(i)\} = 0$, the asymptotic covariance $P_v$ can be shown to be larger than (21).

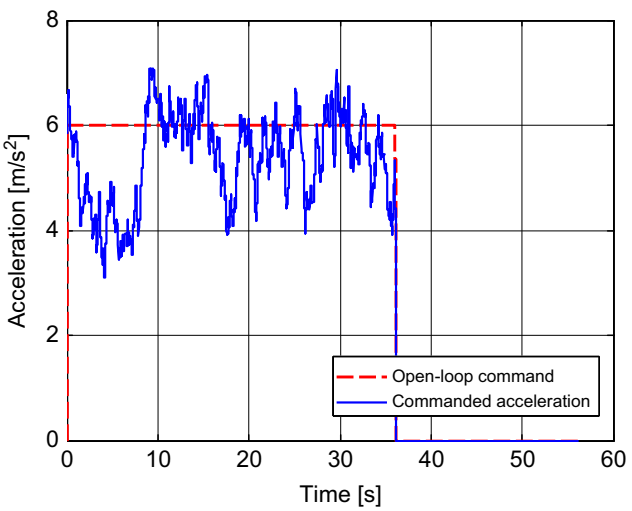


**Fig. 1.** Commanded acceleration.

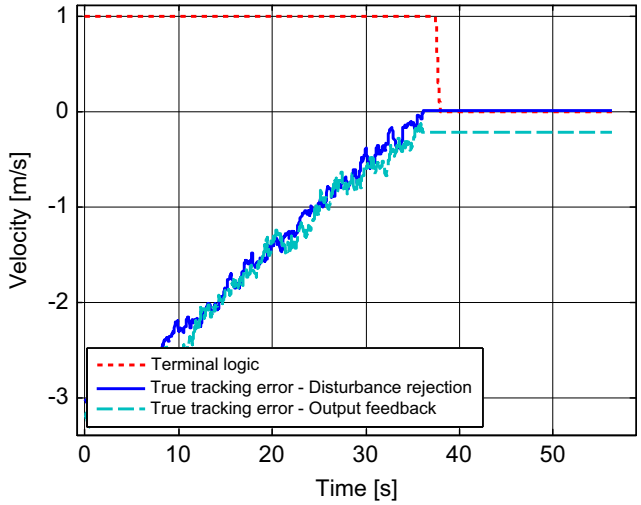


**Fig. 2.** True tracking errors and terminal values.

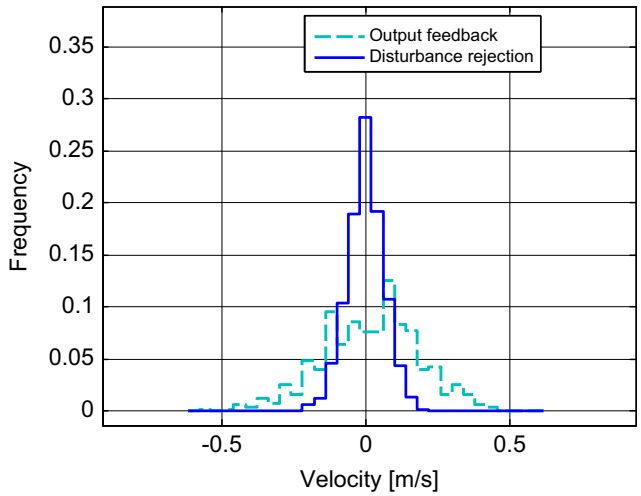


**Fig. 3.** Histograms from 500 Monte Carlo runs.

### 2.6. Monte Carlo results

Monte Carlo runs compare control laws (16) and (27). Control law (16), denoted as 'disturbance rejection' is complemented with state predictors (11) and (14) in order to predict the disturbance state variables. Control law (27), denoted as 'output feedback', employs the raw velocity measurement, which is of no detriment owing to a small measurement noise, on the order of 0.1 m/s ($1\sigma$). A single degree of freedom is reported, i.e. the local vertical velocity, which is distinguished by the subscript $z$. The terminal time $t_f$ is triggered (terminal logic) when the (negative) reference vertical speed reaches zero value, i.e. when $\underline{v}_z \geq 0$. A unique time unit $T=0.05$ s has been assigned to all the control algorithms, which assignment is conservative as the accelerometer sampling time of 10 ms is not exploited.

Fig. 1 shows the commanded acceleration $a_{uz}$ in (16) and the open-loop component $\underline{a}_{uz}$ in (15). The latter which is the sum of the ground Mars gravity $g$ and of a 'constant' braking acceleration, holds

$$\underline{a}_{uz}(i) \cong g + 0.5\underline{v}_z^2(i)/(\underline{h}(i)-\underline{h}(i_f)) \cong 6\,m/s^2, \tag{30}$$

where $\underline{v}_z$ is the vertical velocity, $\underline{h}$ is the altitude and $\underline{h}(i_f) > 0$ the final altitude. The initial altitude $h(0)$ and the initial vertical velocity $v_z(0)$ have been fixed to 1500 m and to $-80$ m/s, respectively.

Fig. 2 compares a pair of realizations of the 'true' tracking error, showing convergence to zero in the 'disturbance rejection' case. Assuming zero bias, i.e. $b_{vz}=0$, the initial 'true' tracking error can be written from (20) as $\underline{v}_z(0)-v_z(0) \cong \underline{e}_{vz}(0)+s_v(v_{dz}(0))$, where $|\underline{e}_{vz}(0)| \leq 3\sigma_v$ is on the order of the velocimeter standard deviation $\sigma_v \cong 0.1\,m/s$, and $|s_v|$ is bounded by $|s_v(v_{dz}(0))| \leq S_{v,\max}$ $|v_{dz}(0)| \cong 3.2\,m/s$. Thus the initial error is dominated by the systematic error $s_v$ as Fig. 2 shows.

In fact, zero convergence of the terminal velocity $v_z(i_f)$ in the 'disturbance rejection' case only occurs in the average as shown by the 500-run histogram by Fig. 3, which corresponds to assuming zero terminal tracking error, i.e. $|\boldsymbol{\varepsilon}|=0$ in (24). Ordinates give the occurrence frequency $n_j/N$, $N=500$, for each abscissa bin $[j-1/2,j+1/2)\Delta x$, where $\Delta x=N/m$ is the bin width and $j=-m/2, \ldots, m/2$. In the 'disturbance rejection' case, the dispersion is only due to the input noise $\mathbf{w}_u$ in (17), but in the 'output feedback' case the not rejected disturbance $\mathbf{d}_s+\mathbf{d}_a$ in (16) makes the difference. Accordingly, the latter case looks more spread, with a root mean square (RMS) value three times larger (0.17 m/s) than the 'disturbance rejection' case (0.06 m/s) and slightly biased as expected from (29). The target RMS is in the order of 0.1 m/s. The velocimeter bias has been fixed at zero.

## 3. Soft landing altitude control

### 3.1. Altitude kinematics and state predictor

The results of Section 2 are briefly extended to the case of altitude control. Accelerometer and velocimeter are now complemented with a radar altimeter, measuring the slanted distance from the vehicle CoM to the terrain along the vehicle axis. Altimeter is assumed to be active also close to the ground, which is usually not the case due to radar limitations. When converted to the local vertical local horizontal frame, the measurement $y_h$ is affected by a systematic error $s_h$, mainly depending on scale factor, misalignment, vehicle tilt and terrain profile, and can be written as

$$y_h(i) = h(i)+s_h(h,\ldots)+e_h(i) = h_d(i)+e_h(i), \tag{31}$$

where $h$ is the local vertical coordinate, $h_d$ is the 'dirty' variable and $e_h(i)$ is the measurement noise on the order of 0.8 m ($1\sigma$). The latter is larger than the equivalent velocimeter noise on the order of $0.1T=0.005$ m ($1\sigma$), which again suggests decoupling between altitude, velocity and acceleration predictors, as in Section 2.

To this end, only kinematic equations are written, namely

$$\begin{aligned} h_d(i+1) &= h_d(i)+v_d(i)+d_h(i)+(p_h(i)+a(i))/2 \\ d_h(i+1) &= d_h(i)+p_h(i)+w_d(i) \\ p_h(i+1) &= p_h(i)+w_p(i) \\ a(i) &= a_u(i)-g(i)T^2+d(i), \end{aligned} \tag{32}$$

where $a_u$ is the commanded acceleration, $g$ is the gravity, $d$ is due to aerodynamics and $T$ has been defined in Section 2.1. In (32) the 2nd order stochastic dynamics providing the

output $d_h$ allows for compensation of velocity and altitude systematic errors. Kinematics in (32) is driven by the 'dirty' velocity $v_d$, by the total acceleration $a$ and by the derivative $p_h$ of the velocimeter systematic error, all expressed in length units.

The total acceleration $a$ and the derivative $p_h$ enter (32) because of discrete-time. As a proof, assuming constant acceleration $a(i)$ during a generic time step $iT \le t < (i+1)T$ and denoting altitude and velocity with $h$ and $v$, the integration of the differential equation

$$\dot{h}(t) = v(t)/T, \quad h(iT) = h(i)$$
$$\dot{v}(t) = (a(t) + p_h(t))/T, \quad v(iT) = v(i), \tag{33}$$

leads to

$$h(i+1) = h(i) + v(i) + a(i)/2$$
$$v(i+1) = v(i) + a(i), \tag{34}$$

whose first equation shows the same form as the uppermost equation of (32). The same occurs to $p_h$.

According to [10] and [11] the noise estimator must include a dynamic feedback, since only a pair of noise components, namely $w_d$ and $w_p$, enter (32) despite three state variables. The fact is that a static feedback could stabilize a closed-loop system around (32) only by adding a third noise component to the first equation of (32). The simplest dynamic estimator holds

$$\begin{bmatrix} w_d \\ w_p \end{bmatrix}(i) = L_h e_h(i) + M_h q_h(i)$$
$$q_h(i+1) = (1-\beta_h) q_h(i+1) + e_h(i), \tag{35}$$

where the gain matrices $L_h$ and $M_h$, and the parameter $\beta_h$ are fixed by four eigenvalues $\lambda_k, k = 1,...,4$. Their design is rather complex as not only must a trade-off be reached between tracking error bias and dispersion, but also between tracking error dispersion and command authority. Slowing the eigenvalues, i.e. pushing $|\lambda_k|$ closer to the unit, decreases dispersion at the price of a higher terminal bias because of a finite time. On the contrary, faster eigenvalues, corresponding to $|\lambda_k|$ much closer to zero, leave measurement noise and model error to affect state variables with the result of a noisy command like the command profile of the 'output feedback' case in Fig. 4.

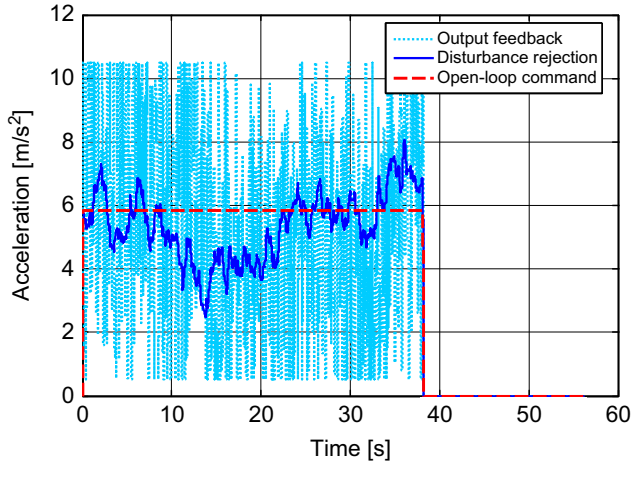


**Fig. 4.** Commanded acceleration for the worst-case altimeter noise (0.8 m, $1\sigma$).

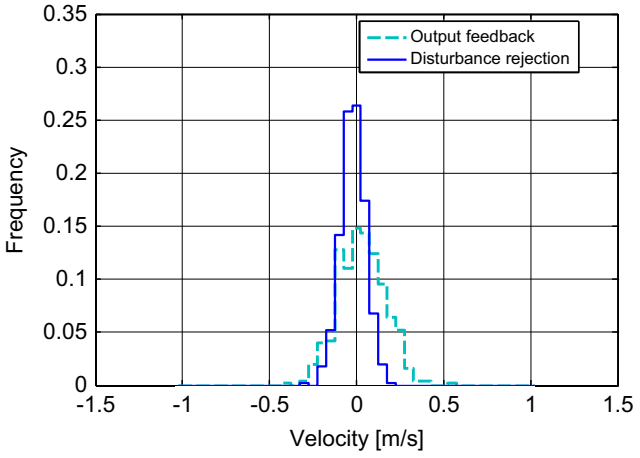


**Fig. 5.** Histograms of the 'true' terminal velocity error for the 25% altimeter noise.

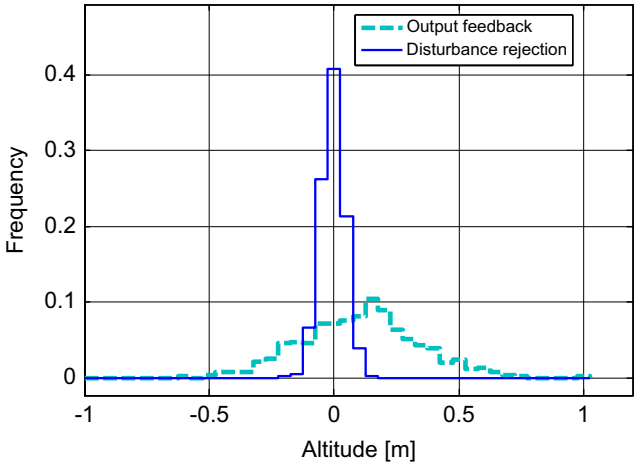


**Fig. 6.** Histograms of the 'true' terminal altitude error for the 25% altimeter noise.

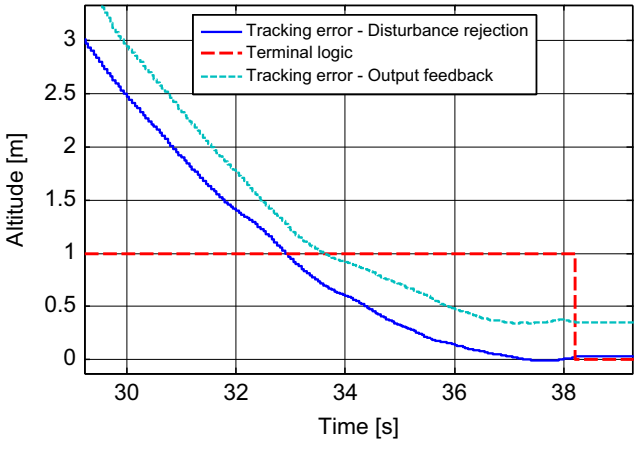


**Fig. 7.** Convergence of the 'true' terminal altitude error.

The control law is similar to (16), except that the 'corrected' velocity tracking error $\underline{e}_v = \underline{v}_z - v_d - d_h$ and the altitude error $\underline{e}_h = \underline{h} - h$ are used, and the systematic error derivative $p_h$ is rejected as follows:

$$a_{uz} = \underline{a}_{uz} + k_h(\underline{h} - h) + k_v(\underline{v}_z - v_d - d_h) - d - p_h. \tag{36}$$

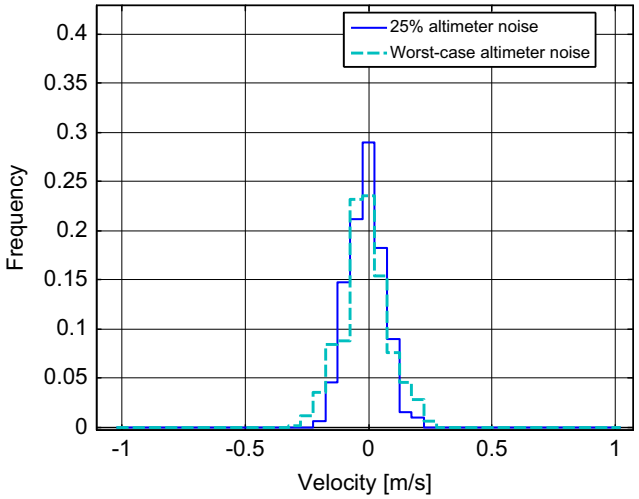


**Fig. 8.** Histograms of the 'true' terminal velocity error for the worst-case and the 25% altimeter noise in the 'disturbance rejection' case.

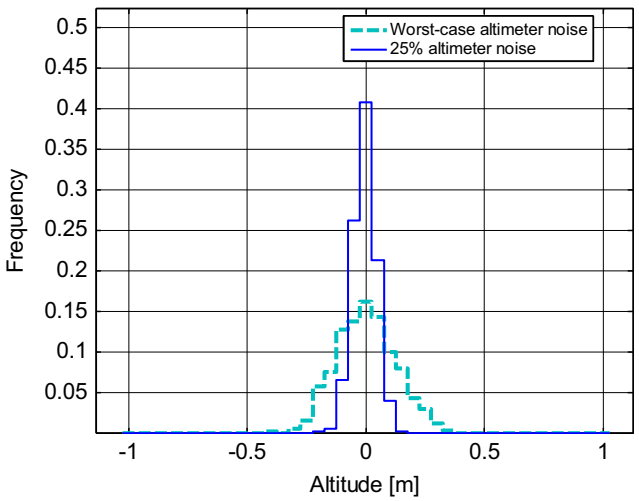


**Fig. 9.** Histograms of the 'true' terminal altitude error for the worst-case and the 25% altimeter noise in the 'disturbance rejection' case.

The output feedback law

$$a_{uz} = \underline{a}_{uz} + k_h(\underline{h} - y_h) + k_v(\underline{v}_z - y_v) \tag{37}$$

is driven by filtered altimeter and velocimeter measures.

Using (32) and (36) similar results to Section 2.4 can be proven.

*Result 7.* If $\lim_{i\to\infty} E\{\underline{e}_h(i)\} = 0$, $\lim_{i\to\infty} \underline{h}(i) = 0$ and $s_h(h = 0) = b_h$, the following limit holds:

$$\lim_{i\to\infty} E(h(i)) = -b_h. \tag{38}$$

The second result accounts for the terminal altitude being close to, but not at, zero, as it depends on the soft landing mechanism employed (crushable structure, legs, air bags and crane [16]). Developing $s_h(h)$ in (31) as $s_h(h) \cong b_h + S_h(\tilde{h})\underline{e}_h$, with $\tilde{h} = \underline{h} - \alpha\underline{e}_h$, $0 \le \alpha \le 1$, and assuming $|S_h(\underline{h} = 0)| \le S_{h,\max} \ll 1$, allows to prove the following result.

*Result 8.* If $|E\{\underline{e}_h(i_f)\}| = \varepsilon$, $\underline{h}(i_f) = h_f > 0$ and $|S_h(|\varepsilon|)| \le S_{h,\max}$, the following inequalities hold:

$$|b_h| - (1 + S_{h,\max})(\varepsilon + h_f) \le |E\{h(i_f)\}| \le |b_h| + (1 + S_{h,\max})(\varepsilon + h_f). \tag{39}$$

### 3.2. Monte Carlo results

The same conditions as in Section 2.6 have been simulated, except for the feedback control gains $k_h$ and $k_v$ in (36) and (37), that have been fixed to appropriate values so that the control law (37) does not saturate the command as a result of a high altimeter noise. To the same goal and to make a fair comparison possible, the RMS of the altimeter noise has been lowered to about 25% (0.2 m) of the typical value of 0.8 m, so that the output feedback control (37) does not saturate the command due to unfiltered measurements. Needless to say, the 'disturbance rejection' law (36), driven by the navigation filter consisting of (32) and of the noise estimator (35) is somewhat insensitive to the worst-case altimeter noise as it can be evinced by comparing the commanded acceleration profiles in Figs. 1 and 4. On the contrary, in the worst-case noise, the output feedback command saturates most of the descent time as Fig. 4 shows.

The Monte Carlo histograms in Fig. 5 show the 'true' terminal velocity has become slightly biased (about 0.02 m/s, absolute value), corresponding to $|\boldsymbol{\varepsilon}| > 0$ in (24), also in the case of the disturbance 'rejection' law (36). The terminal velocity RMS is slightly greater (0.07 m/s) than in the value of 0.06 m/s Section 2.6 because of the altimeter noise. The terminal altitude RMS (Fig. 6) is around 0.05 m compared to the reference altitude of 2 m, which is fully acceptable to any landing mechanism. The terminal error statistics is worse in the 'output feedback' case, becoming biased and widespread as shown in Fig. 5 for the terminal velocity and in Fig. 6 for the terminal altitude. Fig. 7 shows the terminal convergence of the 'true' altitude tracking error; the initial error (outside of Fig. 7) is about 30 m.

To further corroborate the weaker sensitivity to the altimeter noise of the 'disturbance rejection' case, velocity and altitude histograms for the worst-case noise (0.8 m) and for the 25% noise (0.2 m) are compared in Figs. 8 and 9.

The gains of the noise estimator in (35) have been slightly modified from one case to another so as to take the terminal altitude bias close to zero. The amplification factor of the velocity dispersion is about 1.35 in the presence of a noise amplification from 25% to 100%. The amplification of the altitude dispersion through reaching 2.5 remains lower than the fourfold noise factor.

## 4. Attitude control of drag-free satellites

This section is presented without proof. Details can be found in [11] and [17]. An alternative version including neglected dynamics is presented in [12].

### 4.1. State equations and requirements

Drag-free satellites, like the operating Gravity field and steady state Ocean Circulation Explorer (GOCE) [17], need to be accurately aligned to some reference attitude,

which, in the case of GOCE, is given by the local orbit frame, having the first axis aligned with the spacecraft velocity and the second one orthogonal to the current orbit plane. When the spacecraft is low-Earth-orbit (around 300 km in height), the reference quaternion $\underline{\boldsymbol{q}}$ can be obtained from the spacecraft CoM position and velocity vectors provided by on-board GPS (Global Positioning System) receivers. Attitude kinematics can be written in the 'dirty' tracking error $\mathbf{q}_d$ (a three-dimensional vector), defined by the error quaternion

$$\boldsymbol{q}_d = \underline{\boldsymbol{q}}^{-1} \otimes \boldsymbol{q}_s = q_{d0} \begin{bmatrix} 1 & \mathbf{q}_d^T/2 \end{bmatrix}^T, \tag{40}$$

where $\boldsymbol{q}_s = \boldsymbol{q}_I \otimes \boldsymbol{s}_q$ is the product of the inertial quaternion $\boldsymbol{q}_I$ and of the star-tracker systematic error $\boldsymbol{s}_q$. In other terms $\boldsymbol{q}_s$ is the measured quaternion free of random errors. When the error quaternion $\boldsymbol{q}_d$ in (40) can be considered small, the entries $q_{dk}, k = 1,2,3$ of the vector $\mathbf{q}_d$ approximate the 1-2-3 Euler angles, and $\mathbf{q}_d$ can be referred to as the attitude vector. The angular rate error in body coordinates is defined by

$$\Delta\boldsymbol{\omega} = \boldsymbol{\omega} - (\begin{bmatrix} 0 & \underline{\omega} & 0 \end{bmatrix} R(\mathbf{q}))^T, \tag{41}$$

where $\underline{\omega}$ is the angular rate of the orbit frame, $R$ is the body-to-orbit transformation, $\boldsymbol{q} = \underline{\boldsymbol{q}}^{-1} \otimes \boldsymbol{q}_I$ is the 'true' attitude quaternion and $\mathbf{q}$ is the corresponding vector similar to $\mathbf{q}_d$ in (40).

The discrete-time state equations are of the same kind as (32) and (11), and are weakly coupled through gyro and gravity-gradient torques [17].

Only a single generic entry $q_d = q_{dk}$ of the attitude vector $\mathbf{q}_d$ defined in (40) is taken into consideration. Cross-coupling terms are accounted for by a known disturbance term $h$ which is a function of the attitude and rate vectors. Kinematic, dynamic and disturbance state equations take the form

$$\begin{bmatrix} \mathbf{x} \\ \mathbf{d} \end{bmatrix}(i+1) = \begin{bmatrix} A & H \\ 0 & F \end{bmatrix} \begin{bmatrix} \mathbf{x} \\ \mathbf{d} \end{bmatrix} + \begin{bmatrix} B \\ 0 \end{bmatrix} a_u + \begin{bmatrix} G \\ E \end{bmatrix} \mathbf{w} + \begin{bmatrix} N \\ 0 \end{bmatrix} h(\mathbf{q}, \Delta\boldsymbol{\omega}), \tag{42}$$

where

$$\mathbf{x} = \begin{bmatrix} q_d \\ \Delta\omega \\ x_a \end{bmatrix}, \quad \mathbf{d} = \begin{bmatrix} d_s \\ d_a \end{bmatrix}, \quad A = \begin{bmatrix} 1 & 1 & 0 \\ 0 & 1 & 0 \\ 0 & 0 & 0 \end{bmatrix}, \quad F = \begin{bmatrix} 1 & 0 \\ 0 & 1 \end{bmatrix} \tag{43}$$

and

$$N = B = \begin{bmatrix} 1/2 \\ 1 \\ 1 \end{bmatrix}, \quad H = \begin{bmatrix} 1/2 & 1/2 \\ 1 & 1 \\ 0 & 1 \end{bmatrix}, \quad G = \begin{bmatrix} 0 & 0 & 0 & 0 \\ 1 & 0 & 0 & 0 \\ 0 & 0 & 1 & 0 \end{bmatrix}$$

$$\mathbf{w}^T = \begin{bmatrix} w_u & w_s & w_a & w_d \end{bmatrix}, \quad E = \begin{bmatrix} 0 & 1 & 0 & 0 \\ 0 & 0 & 0 & 1 \end{bmatrix}. \tag{44}$$

The entries of $\mathbf{x}$ in (43) are the 'dirty' attitude $q_d$, the rate error $\Delta\omega$, and the 'dirty' acceleration $x_a$, the latter including the systematic error $s_a$ as in (7). The input $a_u$ is the command acceleration to be dispatched to actuators (inertia wheels, thrusters, magnetic torquers). The components of $\mathbf{d}$ and $\mathbf{w}$ have the same meaning as in (11), except that they are now scalars. Specifically, $d_s$ and $d_a$ include opposite values of $s_a$ as in (12). A similar derivation as in Section 3.1 explains the direct contribution of the acceleration terms $a_u$, $d_a$ and $d_s$ to the attitude $q_d$, as shown by the first non zero rows of $B$ and $H$ in (44).

Measurements are provided by ultra-fine accelerometers sampled at 10 Hz and by a single 3D star tracker, sampled at 2 Hz. Accelerometer and star tracker measurements $y_a$ and $y_q$, respectively, are affected by errors and noise as

$$\begin{aligned} y_a(i) &= x_a(i) + e_a(i), \\ y_q(i_k) &= q_d(i_k) + e_q(i_k), \end{aligned} \tag{45}$$

where $i_k = kN_q$, $N_q = T_q/T = 5, T_q = 0.5$ s is the star tracker sampling time, and the systematic errors $s_a$ and $s_q$ are encoded in the 'dirty' variables $x_a$ and $q_d$. The star tracker error is written as $s_q = S_q q + b_q$, sum of scale error and bias.

In drag-free missions, the 'true' attitude, that is $q = q_d - s_q$ must be accurate (aligned with the orbit frame) only in a limited frequency bandwidth, say, above the orbit frequency $f_O \cong 0.2$ mHz (GOCE mission). Accuracy can be expressed either through the (unilateral) spectral density $S_q^2(f)$ of the 'true' attitude, or through the RMS of the attitude in the mission frequency band, say

$$\sigma_q \le \overline{\sigma}_q \le 10\,\mu\text{rad}, \; \sigma_q^2 = \int_{f_0}^{f_1} S_q^2(f) df, \tag{46}$$

where $f_0 = 1$ mHz and $f_1 = 0.1$ Hz are fixed by the mission requirements.

The same applies to the residual acceleration $a = d + u + w_u$ as follows:

$$\sigma_a \le \overline{\sigma}_a \le 50\,\text{nrad/s}^2, \quad \sigma_a^2 = \int_{f_0}^{f_1} S_a^2(f) df. \tag{47}$$

### 4.2. Noise estimator

The noise estimator is decoupled as in the soft landing case, except that only acceleration and attitude are measured rather than the angular rate. Measurement sampling is multi-rate. As shown in [12] and [11], multi-rate noise estimator easily follows from the noise concept of the embedded model: (i) $w_a$ and $w_d$ in (44) are retrieved as in (14) by the model error $e_a = y_a - x_a$, defined in (45), at the faster rate $1/T = 10$ Hz, (ii) $w_u$ and $w_s$ in (44) are set to zero except when attitude measurements are available, i.e. at $i = i_k$. The latter updating process implies that attitude and angular rate in (42) are open-loop propagated between successive star tracker samples as in Kalman filter. The faster noise estimatorof $w_a$ and $w_d$ is static, whereas the slower one, estimating $w_u$ and $w_s$ through the model error $\mathbf{e}_q$ in (45), must be dynamic as in (35), since the size of the noise components is inferior to that of the state variables $q_d$, $\Delta\omega$ and $d_s$ in (43). The complete noise estimator is found to be

$$\begin{aligned} &\begin{bmatrix} w_a \\ w_d \end{bmatrix}(i) = L_a e_a(i) \\ &\begin{bmatrix} w_u \\ w_s \end{bmatrix}(i_k) = L_q e_q(i_k) + M_q p(i_k) \\ &p(i_k + N_q) = \left(1 - \beta_q\right) p(i_k) + e_q(i_k). \end{aligned} \tag{48}$$

The gain vectors $L_a$, $L_q$ and $M_q$ are fixed by the state predictor eigenvalues. The acceleration predictor bandwidth $f_a$ imposed by the gains of $L_a$ in (48) is wider than $f_1$ in (47) ($\geq 0.5$ Hz) so as to accurately retrieve the acceleration disturbance to be rejected. The attitude and rate predictor bandwidth $f_q$ must be narrower than $f_a$ so as to filter the star tracker noise down to the accelerometer level.

A quasi-optimal design (in terms of variance) is pursued by designing the ratio $f_q/f_a$ of the state predictor bandwidths to be bounded by the signal-to-noise ratio $\rho$. The latter is defined as the standard deviation ratio $\rho = \sigma_{aq}/\sigma_q$ between the attitude disturbance $a_q$, which is obtained by doubly integrating the residual acceleration $a = d + u + w_u$, and the star tracker random noise $e_q$ in (45) having standard deviation $\sigma_q \geq 20\,\mu$rad. The standard deviation $\sigma_{aq}$ at the numerator of $\rho$ assumes the residual acceleration bound in (47) and a double integration along a closed-loop time constant $\tau_q \leq 3$ s, which is compatible to the frequency upper bound $f_1$ in (49). As a result the following inequality is obtained

$$f_q/f_a \leq \rho = \overline{\sigma}_a \sqrt{\tau_q^3/3}/\sigma_q \cong 0.0025. \tag{49}$$

Since the bandwidth $f_q \leq 1.5$ mHz of the attitude predictor which results from (49) is rather narrow, gain scheduling has been adopted as in [11]. During the early phase of the accelerometer bias estimation (calibration phase, $t \leq 3000$ s in Figs. 11 and 12) a bandwidth wider than that imposed by (49) is adopted, such to mitigate the attitude drift owing to a partly identified bias (see the onset of Fig.11). As soon as mission accuracy is requested (science phase), the narrow bandwidth imposed by (49) is adopted.

The control law, assuming zero reference for attitude and rate, is computed and dispatched at the faster rate (10 Hz). It is similar to (36) and holds

$$a_u(i) = -k_q q_d - k_\omega \Delta\omega - d_s - d_a - h(\mathbf{q}, \Delta\boldsymbol{\omega}), \tag{50}$$

where $d_s$ cancels the accelerometer bias/drift and $d_a$ cancels disturbance torques due to gravity gradient, aerodynamic forces, the Earth's magnetic field and thruster misalignment. Star tracker scale error has no effect due to zero reference; bias cannot be eliminated.

### 4.3. Simulated results

Simulated runs have been carried out under a simpler spacecraft and in a simpler environment than in [11] and [17]. A single degree of freedom has been simulated, free of cross-coupling. Calibration phase until 3000 s and the subsequent science phase have been simulated. Attitude acquisition to below 1 arcminute is assumed having been performed in a previous phase.

Fig. 10 shows the attitude drift under different versions of the control law (50). The dashed line is obtained by dropping all components in (50) except $d_a$ (disturbance rejection): the drift is due to the accelerometer bias that has been fixed to a small value, 0.1 μrad/s$^2$, to allow for comparison. The dotted line lacks the feedback terms in (50): bias compensation greatly abates the drift, which is now due to acceleration residuals as a result of an imperfect disturbance rejection. The solid line refers to the full control law: attitude is biased because of the star tracker bias around 40 μrad. Fig. 11 proves optimality of

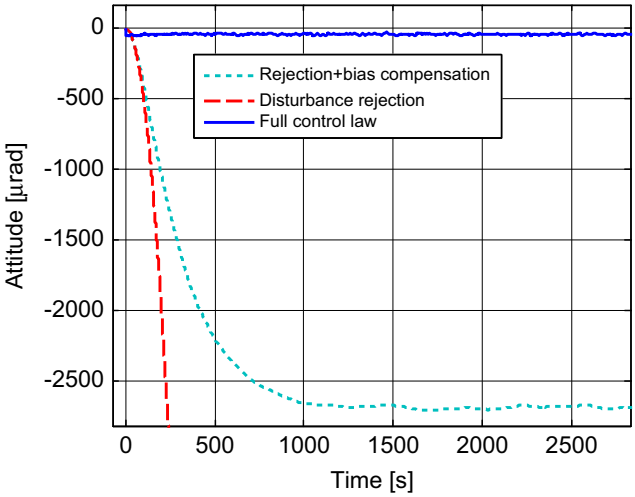


**Fig. 10.** Attitude drift for different control laws.

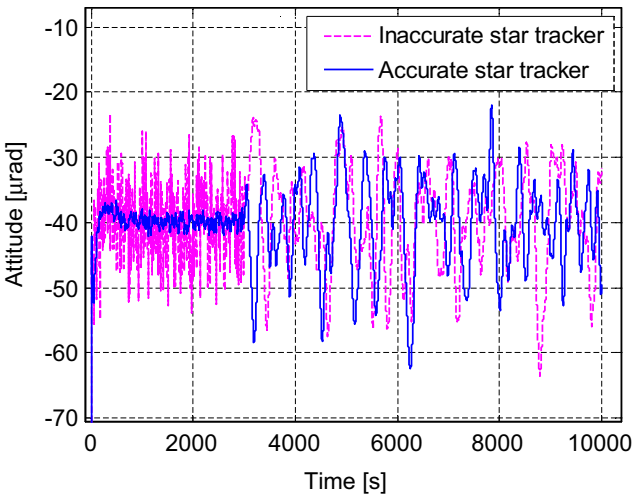


**Fig. 11.** Attitude under different star tracker accuracies.

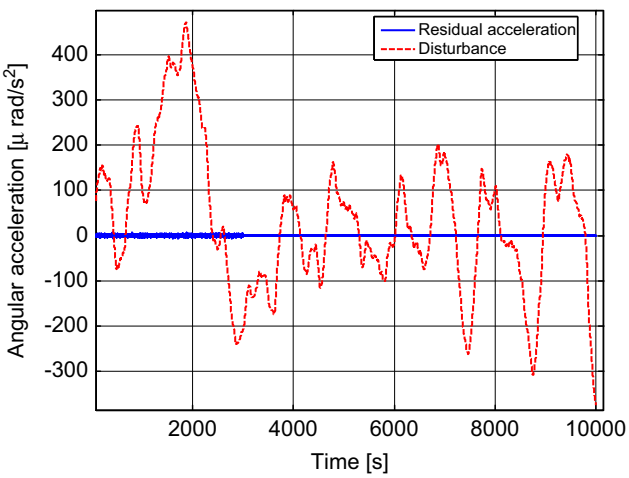


**Fig. 12.** Angular acceleration disturbance and residuals.

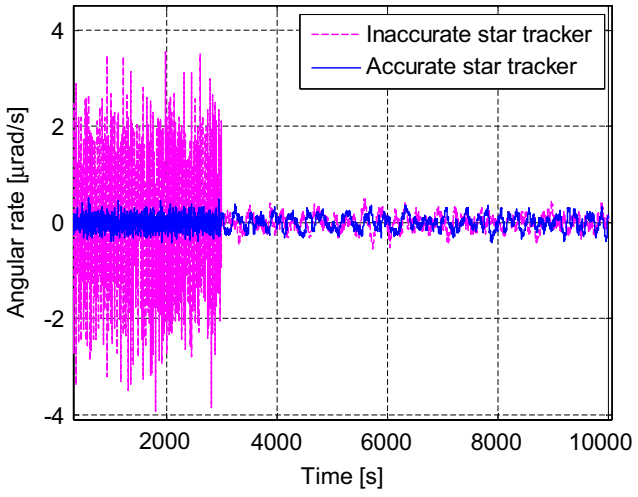


**Fig. 13.** Angular rate under different star tracker accuracies.

the narrow-band noise estimator, as the same attitude RMS, $\leq 10\,\mu\text{rad}$ as requested by (46), is obtained for $t \geq 3000\,\text{s}$ under accurate (dashed line) and inaccurate star trackers. The role of the dynamic noise estimator (second and third rows of (48)) in achieving the target RMS in (46) during the science phase, can be better appreciated from Fig. 13 where the angular rate $\Delta\omega$ is plotted. Indeed, the latter fluctuations appear, as expected, greatly attenuated passing from calibration (wide-band estimator) to science phase (narrow-band estimator) especially in the case of an inaccurate star tracker. The fact is that the spectral density of the angular rate is dominated by mid-frequency components, close to the mission frequency band in (46). On the contrary, integration of the angular rate brings the frequency components below $f_0 = 1\,\text{mHz}$ to dominate the attitude spectral density As a matter of fact attitude fluctuations in Fig. 12 become more widespread but smoother passing from calibration to science phase. Fig. 12 shows the disturbance profile (dashed line) and the residual acceleration (the zero line). The latter RMS satisfies (47) for $t \geq 3000\,\text{s}$, when the narrow-band noise estimator is applied.

## 5. Conclusions

This paper shows how disturbance and noise modeling, as part of the embedded model of a control unit, allows not only the embedding of systematic errors in an appropriate disturbance dynamics in a more generic way than does standard navigation, but also allows us to prove and achieve their real-time compensation. As a consequence, rejection of smooth and trajectory-dependent systematic errors can be feasible also without supplementary sensors, but convergence of the reference trajectory and back-stepping of the error derivative up to command channels are necessary conditions. Supplementary sensors become necessary for the estimation and rejection of DC errors (bias). Disturbance and noise modeling allow to deal with multi-rate measurements, since the driving noise is estimated and the disturbance state variables are updated only at every measurement occurrence. Problem formulation and solutions were illustrated with the help of three study cases taken from space applications.

## Acknowledgments

Part of this research was carried out under the Regional Project STEPS funded by Regione Piemonte (Piedmont Region), Italy and under several contracts with Thales Alenia Space Italia, Turin, Italy within the European ExoMars project. The authors are grateful to Paolo Martella, Thales Alenia Space Italia, for introducing them to the ExoMars landing challenges. The authors also thank two anonymous reviewers for their constructive remarks and suggestions, and Barbara Wade for her linguistic advice.

## References

[1] J. Ospina, E. Canuto, Uncertainty on differential measurements and its reduction using the calibration by comparison method, Metrologia 45 (2008) 389–394.
[2] J. Feng, S. Megerian, M. Potkonjak, Model-based calibration for sensor networks, Proc. IEEE Sensors (2003) 737–742.
[3] R. Tan, G. Xing, X. Liu, J. Yao, Z. Yuan, Adaptive calibration for fusion-based wireless sensor networks, Proc. IEEE INFOCOM (2010) 1–9.
[4] B. Friedland, Treatment of bias in recursive filtering, IEEE Trans. Autom. Control 14 (4) (1969) 359–367.
[5] I. Seo, S. Kang, C.-I. Chang, H. Ko, An efficient bias estimation method in multisensory fusion for navigation by adaptive prototype selection in a bank of Kalman filters, in: Proceedings of the 1999 IEEE International Conference on Multisensor Fusion and Integration for Intelligent Systems, Taipei, Taiwan, August 1999, pp. 279–284.
[6] M.B. Ignagni, Separate-bias Kalman estimator with bias state noise, IEEE Trans. Autom. Control 35 (3) (1990) 338–341.
[7] R. van der Merwe, E.A. Wan, S. Julier, Sigma-point Kalman filters for nonlinear estimation and sensor fusion; applications to inertial navigation, in: Proceedings of the AIAA Guidance, Navigation and Control Conference, Providence, RI, August 16–19, 2004, paper AIAA-2004-5120.
[8] J.B. Hoagg, D.S. Bernstein, Deadbeat internal model control for command following and disturbance rejection in discrete-time systems, in: Proceedings of the 2006 American Control Conference, Minneapolis, MN, June 14–16, 2006, pp. 194–199.
[9] S. Ralhan, T.A. Badgwell, Robust output disturbance rejection for stable systems, in: Proceedings of the 2000 American Control Conference, Chicago, IL, June 2000, pp. 1832–1836.
[10] E. Canuto, Embedded model control: outline of the theory, ISA Trans. 46 (3) (2007) 363–377.
[11] E. Canuto, L. Massotti, A. Molano, Drag-free control of the GOCE satellite: noise and observer design, IEEE Trans. Control Syst. Technol. 18 (2010) 501–509.
[12] E. Canuto, W. Acuna-Bravo, A. Molano-Jimenez, C. Perez-Montenegro, Embedded model control urges disturbance/noise modelling and rejection, in: Proceedings of the 30th Chinese Control Conference, Yantai, China, July 22–24, 2011, pp. 6267–6273.
[13] J.-J.E. Slotine, W. Li, Applied Nonlinear Control, Prentice-Hall Int. Ed., ISBN 0-13-040890-5, 1991.
[14] R.R. Sostaric, J.R. Rea, Powered descent guidance methods for the moon and mars, in: Proceedings of the AIAA GNC Conference and Exhibit, 15–18 August 2005, San Francisco, CA, AIAA 2005-6287.
[15] P. Martella, M. Buonocore, E. Canuto, A. Molano Jimenez, R. Drai, L. Lorenzoni, Design and verification of the GNC for the European ExoMars EDL demonstrator, in: Proceedings of the AIAA Guidance, Navigation and Control Conference, Portland, Oregon, August 8–11, 2011, AIAA 2011-6341.
[16] R.D. Braun, R.M. Manning, Mars Exploration Entry, Descent and Landing Challenges, IEEEAC paper 0076, December 2005.
[17] E. Canuto, Drag-free and attitude control for the GOCE satellite, Automatica 44 (7) (2008) 1766–1780.